J. Fluid Mech. (1975), *vol.* 67, *part* 4, *pp.* 667–687
Printed in Great Britain

Parametric instability of internal gravity waves

By A. D. McEWAN AND R. M. ROBINSON
CSIRO Division of Atmospheric Physics, Aspendale, Victoria 3195, Australia

(Received 3 December 1973 and in revised form 20 May 1974)

A continuously stratified fluid, when subjected to a weak periodic horizontal acceleration, is shown to be susceptible to a form of parametric instability whose time dependence is described, in its simplest form, by the Mathieu equation. Such an acceleration could be imposed by a large-scale internal wave field. The growth rates of small-scale unstable modes may readily be determined as functions of the forcing-acceleration amplitude and frequency. If any such mode has a natural frequency near to half the forcing frequency, the forcing amplitude required for instability may be limited in smallness only by internal viscous dissipation. Greater amplitudes are required when boundaries constrain the form of the modes, but for a given bounding geometry the most unstable mode and its critical forcing amplitude can be defined.

An experiment designed to isolate the instability precisely confirms theoretical predictions, and evidence is given from previous experiments which suggest that its appearance can be the penultimate stage before the traumatic distortion of continuous stratifications under internal wave action.

A preliminary calculation, using the Garrett & Munk (1972*a*) oceanic internal wave spectrum, indicates that parametric instability could occur in the ocean at scales down to that of the finest observed microstructure, and may therefore have a significant role to play in its formation.

1. Introduction

In nature, the tendency for wavelike motions of all scales to lose their coherence is well known. In many circumstances weak waves (gravitationally or rotationally restored) are demonstrably 'stable' in the sense that their form is invariant with time or dispersion, yet when they are permitted to grow to some finite amplitude their identity is rapidly lost, with or without the accompaniment of 'turbulence' (indeed, the title of turbulence may reflect not so much the intrinsically random nature of the resultant structure but its apparent complexity).

Some use has been made of conventional stability criteria applied to *localities* within the wave field in order to predict the onset of finite amplitude instability. For internal waves in a continuously stratified medium, Orlanski (1972), for example, adopted a criterion for static gravitational instability, $\nabla\rho.\mathbf{g} < 0$ (ρ = density, $\mathbf{g}$ = gravitational acceleration), and found that, until this condition was reached, standing wave motion remained describable by the inviscid equations of motion. Well before that stage was attained, however, the initially simple wave field became profoundly modulated by fine-structure (apparently neglected

by Orlanski in deriving his kinematic expressions for the critical wave amplitude). His figure 5 shows this clearly, and entirely similar effects have been seen elsewhere, e.g. McEwan (1971, figure 7 *d*). There is little doubt that these modulations were major contributors to the eventual state of static instability.

In experiments on the forced interaction of a pair of internal wave beams (McEwan 1973) fine-scale distortion was detected when the isopycnic slope was large, but significantly short of that required for static instability.

Static instability is unquestionably a primary mechanism for the production of 'true', statistically random turbulence within a stratified medium, because it results in the rapid and irreversible growth of disturbances of small scale. It is important to realize, however, that this state is commonly the *end result of the evolution of a more sensitive but slower developing instability of the original motion.*

A particularly ubiquitous instability of this kind is due to resonant interaction. For internal waves the process is of second order, so that instability can develop upon a dominant wave by the amplification (from background noise) of a *pair* of parasitic free wave modes which form a resonant triad with the dominant wave. It has been found (McEwan 1971; Martin, Simmons & Wunsch 1972; McEwan, Mander & Smith 1972) that, even in bounded motions, the resonant triads are numerous and the wave amplitude for instability is small.

In spite of a predisposition towards resonantly interactive instability, the slowness with which this develops when triad members have to grow from small levels could mean that in real situations less sensitive but more rapidly acting processes will dominate. The fact that the internal wave spectrum (though not heavily populated by resonant triads) is usually dense leads naturally to the conjecture that there might commonly occur an unstable interaction between *pairs* of waves having suitable properties.

Such an interaction would involve the forcing of one of the waves at the frequency of the other wave (the natural frequencies in general being unequal). Time dependence is thus expressed by a differential equation containing periodic coefficients. Under circumstances where spatial periodicity constraints can be relaxed this takes the form of the Mathieu equation, and the process is recognizably a parametric instability.

Numerous applications of this equation arise in mechanics and physics (see, for example, Brillouin 1953). Parametric resonance shows itself in the excitation of subharmonic surface waves through vertical acceleration (Benjamin & Ursell 1954), edge waves (Bowen & Inman 1969) and cross-waves (Garrett 1970; Mahony 1972). Rhines (1970) derived dispersion relations and applied these to an internal wave in a sinusoidal shear flow and Orlanski (1973) suggested that diurnal changes in stability could parametrically excite internal gravity waves in the atmosphere. Very little attention, however, appears to have been given in the case of stratified media to parametric excitation through the presence of concurrent waves, although this can be regarded as a degenerate example of the much-studied processes of resonant wave interaction.

This paper presents the basic theory (§2) and experiments (§§3 and 4) to verify the process in its simplest form. It is shown that a periodic rotation of the isopycnics of a uniform stable stratification, as imposed by a large-scale plane

internal wave, is liable to yield instability tending to produce density perturbations of finer spatial scale, and at an angle to the horizontal shallower than the characteristic angle of the large-scale wave. Present and previous observations (§5) suggest that these perturbations are the penultimate stage in the formation of an irreversible 'traumatic' distortion of a continuous density field. Using the Garrett & Munk (1972*a*) spectrum, a simplified examination of possible application to oceanic internal wave structure is made (§6). From this, parametric instability seems likely to occur in waves of scales down to that of the finest observed microstructure.

2. Theory

2.1. *Parametric instability in a locally uniform background oscillation*

The simplest illustration of the mechanism of parametric instability in a stratified fluid arises in the case when the unstable mode has a scale very much smaller than the scale of the background motion on which it grows.

Consider the motion of a fluid element within a body of stably stratified fluid under the action of a large-scale motion. We adopt a co-ordinate frame (x, z) fixed relative to this element; the frame then undergoes translation and rotation through an angle $\alpha(t)$ to the horizontal so that its x axis remains aligned with the isopycnal surface $\rho_0(0, t) =$ constant. The density $\rho_0(x, z, t)$ is defined only by the large-scale field, and the pre-existing static stratification, whose vertical gradient is denoted by ρ'_{00}, taken to be locally constant. This density field is perturbed by fine-scale motion (u, w) of dimensionless magnitude $o(\epsilon)$, resulting in a net density given by

$$\rho_1 = \rho(x, z, t) + \rho_0 + \rho_{00}$$

and net motion $u_1 = u_0 + u$, $w_1 = w_0 + w$, in the frame (x, z).

The equation for momentum relative to a moving frame is

$$\rho\left(\frac{D\mathbf{u}}{Dt} - \mathbf{F} + \mathbf{a}_0 + 2\boldsymbol{\Omega}\times\mathbf{u} + \frac{d\boldsymbol{\Omega}}{dt}\times\mathbf{x} + \boldsymbol{\Omega}\times(\boldsymbol{\Omega}\times\mathbf{x})\right) = -\nabla p + \rho\nu\nabla^2\mathbf{u},$$

where $\mathbf{a}_0$ and $\boldsymbol{\Omega}$ are, respectively, the absolute acceleration and rotation rate of the frame, $\mathbf{F}$ is the body force and the other terms have their usual meaning. In the present case, this resolves to

$$\left.\begin{aligned} \rho_1(Du_1/Dt + \ddot{a} - 2w\dot{\alpha} - z\ddot{\alpha} + x\dot{\alpha}^2) &= -\partial p/\partial x - \rho_1 g\sin\alpha + \rho_1\nu\nabla^2 u_1, \\ \rho_1(Dw_1/Dt + \ddot{b} + zu\dot{\alpha} + x\ddot{\alpha} + z\dot{\alpha}^2) &= -\partial p/\partial z - \rho_1 g\cos\alpha + \rho_1\nu\nabla^2 w_1, \end{aligned}\right\} \tag{2.1}$$

where $\ddot{a}$ and $\ddot{b}$ are components of the absolute acceleration of the element in the x and z directions.

Continuity and mass conservation require that

$$D\rho_1/Dt = 0, \quad \partial u_1/\partial x + \partial w_1/\partial z = 0. \tag{2.2}$$

If the large-scale motion is a plane internal wave of horizontal and vertical wavenumbers k_0 and m_0, and frequency ω_0, its amplitude may be defined in

terms of α; with capitals denoting components relative to a stationary frame (X, Z),

$$U_0 = -\alpha(X, Z, t)\omega_0 m_0/k_0^2, \quad W_0 = \alpha(X, Y, t)\omega_0/k_0$$

and

$$P_0 = \dot{\alpha}(X, Z, t)\rho'_{00}/\omega_0 k_0,$$

etc., to second order in α, where

$$\alpha(X, Z, t) = \alpha_M \exp\{i(k_0 X + m_0 Z + \omega_0 t)\}.$$

Locating the mean position of the (x, z) frame origin on $X = 0$, $Z = 0$, the field can be rewritten relative to this frame, and substituted in (2.1) and (2.2). The resulting expressions contain terms of ascending order in α, x and z, but if we confine our attention to terms of first order in α and ϵ and to x and z scales very much less than k_0^{-1} and m_0^{-1}, (2.1) and (2.2) combine to give

$$\frac{\partial}{\partial t}\left(\frac{\partial u}{\partial z} - \frac{\partial w}{\partial x}\right) - \ddot{\alpha}\left(\frac{m_0^2}{k_0^2} + 1\right) = \frac{g}{\rho_{00}}\left(\frac{\partial \rho}{\partial x}\cos\alpha - \frac{\partial \rho}{\partial z}\sin\alpha\right) + \nu\left(\frac{\partial \nabla^2 u}{\partial z} - \frac{\partial \nabla^2 w}{\partial x}\right)$$
$$- \frac{\rho'_{00}}{\rho_{00}}\left(g\sin\alpha - \frac{\omega_0 m_0}{k_0^2}\dot{\alpha}\right), \quad (2.3)$$

$$\partial\rho/\partial t + \rho'_{00} w = 0, \quad (2.4)$$

$$\partial u/\partial x + \partial w/\partial z = 0. \quad (2.5)$$

The term $(\omega_0 m_0/k_0^2)\dot{\alpha}$ in (2.3) arises from horizontal accelerations imposed by the large-scale field. These become significant only as $\omega_0^2 m_0/k_0^2 \sim g$; with the dispersion relation (2.7) this implies that $\rho'_{00} m_0 \sim \rho_{00}(m_0^2 + k_0^2)$, i.e. a field which has a vertical scale comparable with the density scale length. In most situations this is an unlikely condition; furthermore the term due to the vertical acceleration of the large-scale field is $O(\alpha^2\omega_0^2/k_0)$ and does not assume significance unless $\alpha \sim m_0/k_0$, in which case gross nonlinearities are already present. To all practical intents, therefore, gravity imposes the only important body force.

From (2.3) the angular displacement due to the large-scale mode satisfies

$$\ddot{\alpha} + [N^2 k_0^2/(k_0^2 + m_0^2)]\sin\alpha = 0, \quad (2.6)$$

which is the equation for small amplitude motion of a simple pendulum with a frequency ω_0 complying with the inviscid dispersion relation for internal waves

$$(\omega_j/N)^2 = k_j^2/(k_j^2 + m_j^2) = (1 + l_j^2)^{-1}, \quad (2.7)$$

where $l_j \equiv m_j/k_j$ is the cotangent of the characteristic angle β_j of wave mode j, and $N = -g\rho'_{00}/\rho_{00}$, the buoyancy frequency.

The foregoing equations become accurate to large α if the large-scale mode is a standing wave whose vertical and horizontal wavenumbers are equal; then, by (2.7), $\omega_0 = N/2^{\frac{1}{2}}$ and, in the vicinity of the origin, the motion approximates to what will be called henceforth the basic (cylindrical) mode, a circular solid-body rotation about the origin. In stream-function terms this has the form

$$\Psi = N\alpha_M 2^{\frac{3}{2}}(X^2 + Z^2)\cos(Nt/2^{\frac{1}{2}}), \quad (2.8)$$

where α_M is the maximum angular displacement.

Combining (2.3) and (2.6) the disturbance-mode density equation becomes

$$\frac{\partial^2}{\partial t^2}(\nabla^2\rho) - \nu\nabla^4\frac{\partial\rho}{\partial t} - N^2\left(\frac{\partial^2\rho}{\partial x\,\partial z}\sin\alpha(t) - \frac{\partial^2\rho}{\partial x^2}\cos\alpha(t)\right) = 0. \tag{2.9}$$

The time factor in solutions to this equation in the form $\rho = R(t)\exp i(kx+mz)$ satisfies the equation

$$\ddot{R} + \nu k^2(1+l^2)\,\dot{R} - N^2(l\sin\alpha(t) - \cos\alpha(t))\,R/(1+l^2) = 0, \tag{2.10}$$

with l as defined above.

By the substitution

$$S = R\exp\{\tfrac{1}{2}\nu k^2(1+l^2)t\} \tag{2.11}$$

equation (2.10) is rewritten as

$$\ddot{S} - [N^2(l\sin\alpha(t) - \cos\alpha(t)) + \tfrac{1}{4}\nu^2k^4(1+l^2)^3]\,S/(1+l^2) = 0. \tag{2.12}$$

This second-order equation with periodic coefficients possesses solutions of the form $S(t) = e^{\mu t}F(t)$, where $F(t)$ has the same periodicity as α; for small α's, $\alpha(t) \approx \alpha_M\cos(\omega_0 t)$ and the equation can be simplified to the standard form of the Mathieu equation,

$$d^2S/ds^2 + (A - 2Q\cos 2s)S = 0, \tag{2.13}$$

by the substitutions

$$\left.\begin{aligned} s = \tfrac{1}{2}\omega_0 t, \quad A &= 4[-\tfrac{1}{4}\nu^2k^4(1+l^2) + N^2](1+l^2)^{-1}\omega_0^{-2}, \\ Q &= 2N^2l^2\alpha_M\omega_0^{-2}(1+l^2)^{-1}. \end{aligned}\right\} \tag{2.14}$$

The properties of this equation are well documented (see Abramowitz & Stegun 1965). Floquet solutions have the form $S(s) = e^{\pm i\mu s}F_\mu(\pm s)$, where $\cos\pi\mu = S_1(\pi)$ and S_1 satisfies (2.13) with $S_1(0) = 1$ and $S_1'(0) = 0$. These solutions are generally linearly independent and divide the $A^{\frac{1}{2}}$, $2Q/A$ plane, see figure 1, into regions of instability (μ complex) and stability (μ real). In unstable regions contours of constant $e^{i\mu\pi}$ are closest to the A axis in the vicinity of $A^{\frac{1}{2}}$ = an integer, so that, for a given growth exponent, Q (and therefore α_M) reaches a minimum for specific values of l. Therefore the perturbations growing upon a wave field of frequency ω_0 will tend to be (neglecting small viscous terms in A) aligned at an angle to the constant density surfaces of

$$\operatorname{arcot} l = \pm\arcsin(I\omega_0/N2^{\frac{1}{2}}), \tag{2.15}$$

where I is an integer $\geqslant 1$.

If part of a solution $S(s)$ represents a free wave mode whose frequency ω is given by (2.7)† then for the most unstable modes, by substitution in (2.15),

$$\omega \pm \tfrac{1}{2}I\omega_0 < N. \tag{2.16}$$

The correspondence between the foregoing process and resonant interaction in weakly nonlinear systems is evident. For $A^{\frac{1}{2}}$ near 1,

$$i\mu = i + \operatorname{Re}(i\mu)$$

and for small Q the growing Floquet solution has the form

$$S(s) = \exp\{\operatorname{Re}(i\mu)s\}\{C_{-2}e^{-is} + C_0e^{is} + O(Q)\} \tag{2.17}$$

† Near $A^{\frac{1}{2}} = I$ there are constraints on the relative magnitudes of 'free' and 'forced' components of $S(s)$; see Rhines (1970).

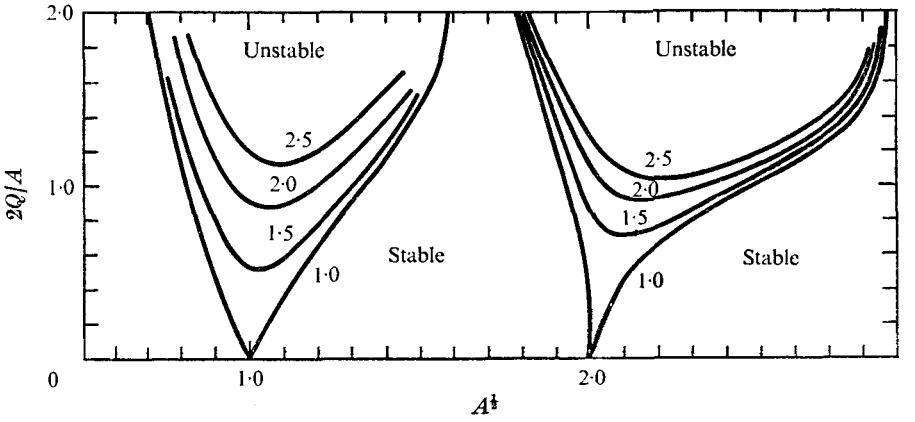

FIGURE 1. Contours of constant $\mathrm{Re}(e^{i\mu\pi})$, in unstable regions. The figure is abstracted from figures 20.8 and 20.9 of Abramowitz & Stegun (1965).

(cf. Abramowitz & Stegun 1965, equation 20.3.8 with $\nu \equiv \mu$ and $z \equiv s$). A resonant triad is made up of the basic motion and the wave components

$$C_{-2}\exp\{-i(\tfrac{1}{2}\omega_0 t - kx - mz)\}, \quad C_0\exp\{i(\tfrac{1}{2}\omega_0 t + kx + mz)\},$$

indicating that $I = 1$ corresponds to a second-order resonant interaction. Similarly the cases $I = 2$ and 3 correspond to third- and fourth-order resonant interactions, the interacting components being themselves products of forced interaction. Their rates of growth are correspondingly smaller, and of course in the present application terms of higher order in α would have to be retained. If the modes within a system are predetermined or restricted by boundaries and are, when interacting, incapable of satisfying an exact resonance condition, then the capacity for the unstable growth of one mode under the periodic excitation of another is determined by the appropriate $\mu(Q, A)$. By (2.11), if

$$\mathrm{Re}\,(i\mu(Q,A)) > \nu k^2(1+l^2)/\omega_0 \tag{2.18}$$

unstable growth will occur. In a bounded, spatially non-uniform large-scale wave field of volume V through which the perturbation can disperse uniformly, the instability condition is evidently

$$\mathrm{Re}\left(2i\int_V \mu(Q,A)\,\omega_0 E\,dV\right) > \text{net energy dissipation rate},$$

where E is the energy contained in the unstable mode per unit volume. Dissipation at the boundaries may contribute to the net dissipation.

2.2. *Application to the instability of a basic cylindrical mode in a real contained fluid*

The cylindrical mode (2.8) is particularly appropriate for experimental investigation for two reasons.

(i) Motion terms relative to the axis of rotation, U and W, and the particle accelerations $\ddot{a}$ and $\ddot{b}$ disappear, and the modal wavenumber is zero, so (2.9) is accurate to second order in α.

(ii) Boundaries to the mode are cylindrical; hence (except for viscous effects) there occurs no excitation of spurious high wavenumber disturbances through the forcing of the mode.

The natural modes for a uniform stratification within a cylindrical boundary $x^2+z^2-a^2=0$ and conforming to the first-order equation for the perturbation stream function

$$\nabla^2\psi_{tt}+N^2\psi_{xx}=0 \tag{2.19}$$

have been determined by Barcilon (1968) in the analogous context of inertial waves. For the present purpose they can be written as

$$\psi^{(j)}_{MK}=A^{(j)}_{MK}[T_{mK}(\xi_{MK}/a)-(-1)^{jK}T_{jK}(\xi_{MK}/a)]\exp(iN\cos\beta_{MK}t), \tag{2.20}$$

where $\beta_{MK}=\frac{1}{2}\pi M/K$ (M and K mutually prime integers, $K<M$),

$$\xi_{MK}=x\cos\beta_{MK}+z\sin\beta_{MK},$$
$$\zeta_{MK}=x\cos\beta_{MK}-z\sin\beta_{MK}$$

and T_{jK} is the Chebyshev polynomial or order jK, $T_{jK}(x)=\cos(jK\cos^{-1}x)$. $A^{(j)}_{jK}$ is the amplitude in stream-function units. There exists a doubly infinite countable set of eigenfrequencies $N\cos\beta_{MK}$, and for each frequency there is a countably infinite set of eigensolutions or modes $\psi^{(j)}_{MK}$. However, in a real fluid the higher modes are suppressed by viscosity.

In systems of modest scale viscous dissipation at the boundaries far exceeds that in the interior. The total dissipation within the boundaries is

$$\rho\nu\iiint(\nabla\times\mathbf{u})^2\,dV. \tag{2.21}$$

To a close approximation, the interior dissipation D_I is determined by integrating the inviscid field to the boundaries, i.e.

$$D_I=\frac{\rho\nu b}{2}\iint_{x^2+z^2<a^2}(\nabla^2\psi^{(j)}_{MK})^2\,dx\,dz, \tag{2.22}$$

where b is the cylinder breadth.

The boundary-layer scale and therefore the dissipation depend on the angle θ of the boundary to surfaces of constant density in the interior. The dissipation can be estimated by assuming that locally this angle is constant and effects of velocity gradients in the direction parallel to the boundary may be neglected; then the boundary-layer motion is given, on the end walls $y=0$, b (see, for example, McEwan 1971), by

$$\left.\begin{aligned}u&=u_i[\cos\omega t-e^{-\zeta}\cos(\omega t-\zeta)],\\ w&=w_i[\cos\omega t-e^{-\xi}\cos(\omega t+\xi)].\end{aligned}\right\} \tag{2.23}$$

(u_i, w_i) is the interior motion and

$$\zeta=\frac{1}{2^{\frac{1}{2}}}\left(\frac{N\cos\beta_{MK}}{\nu}\right)^{\frac{1}{2}}\gamma,$$
$$\xi=\frac{1}{2^{\frac{1}{2}}}\left(\frac{N\cos\beta_{MK}}{\nu}\right)^{\frac{1}{2}}\left(\frac{1}{\cos^2\beta_{MK}}-1\right)^{\frac{1}{2}}\gamma,$$

where γ is the interior-directed normal co-ordinate.

On the cylindrical walls the tangential velocity component q ($q^2 = u^2 + w^2$) is

$$q = q_i[\cos\omega t - e^{-\xi}\cos(\omega t + d\xi)], \tag{2.24}$$

where

$$\xi = \frac{1}{2^{\frac{1}{2}}}\left(\frac{N\cos\beta_{KM}}{\nu}\right)^{\frac{1}{2}}\left|\frac{\cos^2\theta}{\cos^2\beta} - 1\right|^{\frac{1}{2}},$$

$$d = \pm 1, \quad \cos^2\theta \lesseqgtr \cos^2\beta_{MK}.$$

This expression is not valid near the singular points $\cos^2\theta = \cos^2\beta_{MK}$ but gives a reliable (although slightly overestimated) value of the total dissipation. Substituting the above in (2.21) and integrating over time gives, in the mean:

$$\text{end-wall dissipation } D_E = 2^{\frac{1}{2}}\rho(\omega\nu)^{\frac{1}{2}}(l\cos^2\beta + \sin^2\beta)A_{MK}^{(j)2}(jK)^2\pi, \tag{2.25}$$

$$\text{circular-wall dissipation } D_C = \rho\frac{b}{a}(\omega\nu)^{\frac{1}{2}}\frac{A_{MK}^{(j)2}(jK)^2}{2^{\frac{3}{2}}}\int_0^{2\pi} f^2(\theta)\left|\frac{\cos^2\theta}{\cos^2\beta} - 1\right|^{\frac{1}{2}} d\theta, \tag{2.26}$$

where

$$f(\theta) = \left[\frac{\sin[jK(\theta-\beta)]\cos(\theta-\beta)}{\sin(\theta-\beta)} - (-1)^{jM}\frac{\sin[jK(\theta+\beta)]\cos(\theta+\beta)}{\sin(\theta+\beta)}\right],$$

$l = \tan\beta$ and $\omega = N\cos\beta$. Here $\beta \equiv \beta_{MK}$. The total mean energy of the mode is

$$E = \tfrac{1}{2}\rho\iiint[\psi_x^2 + \psi_z^2]\,dV = \rho b A_{MK}^{(j)2}(jK)^2\pi$$

and the rate of viscous attenuation can be determined by equating dE/dt to $D_I + D_E + D_C$ as determined above; thus without forcing, the amplitude of an individual mode is

$$A_{MK}^{(j)} = A_{MK}^{(j)}(t=0)\,e^{-\kappa^* t},$$

where

$$\kappa^* = (D_I + D_E + D_C)/2E. \tag{2.27}$$

From (2.20) the basic cylindrical mode has the form

$$\psi_{12}^{(1)} = A_{12}^{(1)}\left[T_2\left(\frac{\xi}{a}\right) + T_2\left(\frac{\zeta}{a}\right)\right]\cos\frac{Nt}{2^{\frac{1}{2}}} = \frac{2A_{12}^{(1)}}{a^2}(x^2 + z^2 - a^2)\cos\frac{Nt}{2^{\frac{1}{2}}},$$

cf. (2.8). The accuracy of the above dissipation formulae was tested by measuring experimentally the rate of decay of this mode, using the apparatus and methods to be described in §3. Figure 2 shows a comparison of the observed decay in amplitude after cessation of the 'horizontal' method of forcing with the rate predicted by (2.27) using appropriate values for N and ν. Agreement of the mean κ^* is to within better than 3 %, with the theoretical estimate slightly higher, as expected.

Knowledge of the decay rate of specific modes is necessary in order to identify which of these is most unstable to parametric excitation. For bounded systems it has proved justifiable (e.g. McEwan 1971) to replace the internal dissipation within an unstable mode by its total dissipation; thus in the condition for instability (2.18) the right-hand side is replaced by κ^*, i.e.

$$\mathrm{Re}\,(\tfrac{1}{2}i\mu(Q, A)\,\omega_0) \geqslant \kappa^* \tag{2.28}$$

for instability.

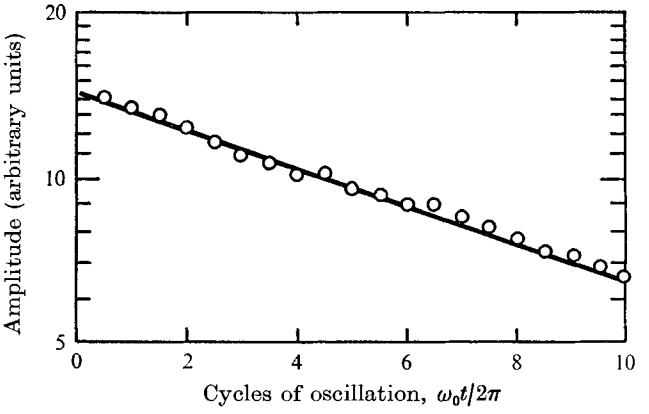

FIGURE 2. Comparison of predicted and observed viscous damping rates for the basic cylindrical mode. ○, experiment at half-cycle intervals; ——, theoretical prediction, equation (2.27).

3. Design and conduct of the experiment

As pointed out in §2.2, a horizontal circular cylinder is probably the most convenient boundary geometry for experimental verification of parametric instability. An additional advantage is that, in the absence of a forced spatial structure for the basic mode, low-order *resonant* interaction cannot occur, therefore permitting the unambiguous detection of off-resonant parametric instability.

Hence the following arrangement was adopted. Reference is made to figure 3. The test chamber was a right circular cylinder with plane ends of radius 15·24 cm and 22·9 cm long. This fitted neatly into a rectangular tank with parallel plate-glass sides 22·9 cm apart, such that the cylinder axis lay horizontal and central within the tank. The edges of the cylinder were sealed against the glass with modelling clay. Filling holes, 2·5 cm in diameter with vertical axes in the mid-plane of the cylinder, had shaped silicone rubber plugs which could be pushed home by handles outside the tank, to present a smooth cylindrical surface on the inside of the chamber. Skirts extending nearly to the top and bottom of the tank surrounded the filling holes. The tank had a watertight lid, and could be completely filled through a mushroom opening in the bottom, after opening the plugs and a bleed hole in the lid.

It turns out that, in the arrangement described, if the density of the liquid (in our case, salt-stratified water) increases linearly with the volume admitted, a linear stratification is attained within both the tank *and* the test chamber, provided that the chamber axis is on the central plane of the tank, the chamber is symmetrical about that plane and the tank is completely filled. The skirts surrounding the filling holes were needed to avoid undesirable mixing which occurred as the liquid levels reached these holes.

In practice, the density–volume relation was established using the two-tank method of filling; the chamber density gradient was accurately linear except in the top and bottom 10 % or so of the depth, where it weakened monotonically,

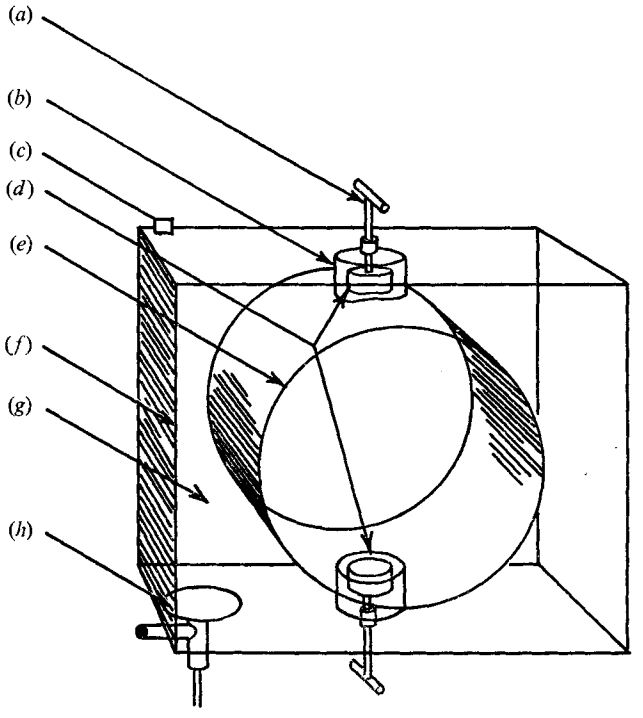

FIGURE 3. Experimental chamber. (*a*) Plug handle. (*b*) Skirt. (*c*) Bleed hole plug. (*d*) Silicone rubber plugs. (*e*) Cylindrical chamber. (*f*) Rectangular tank. (*g*) 0·63 cm plate-glass sides. (*h*) Filling mushroom.

apparently because of mixing at the holes, which occurred when the free surfaces met just as filling was completed. A test profile is given in figure 7.

The reason for using a cylindrical chamber was that the fluid could be set into a pendulum mode of solid-body oscillation, the boundaries then exciting no other modes. The forcing acceleration was thus uniform throughout the volume. Furthermore, possible interacting modes were constrained in structure by the boundaries and, as indicated in §2.2, were limited by the requirement that, from (2.20),

$$\arccos \omega/N = \pi M/2K,$$

where for high K and M dissipation becomes dominant.

Two methods for initiating the basic, solid-body oscillation were attempted.

For the first method (I), the whole assembly was mounted upon a frame which hung from a pair of horizontal sliding-door tracks (see figure 4*a*). After first determining the natural frequency of the solid-body rotation mode, the assembly was pushed smoothly to and fro through a distance of up to 3 m several times at this frequency, and then observed by arresting it within the beam of a schlieren optical system incorporating two *f* 8 spherical mirrors 31 cm in diameter. Owing to the abruptness of the forcing procedure, the initial transient oscillations, though small in amplitude, were abundant, and identifiable instabilities appeared

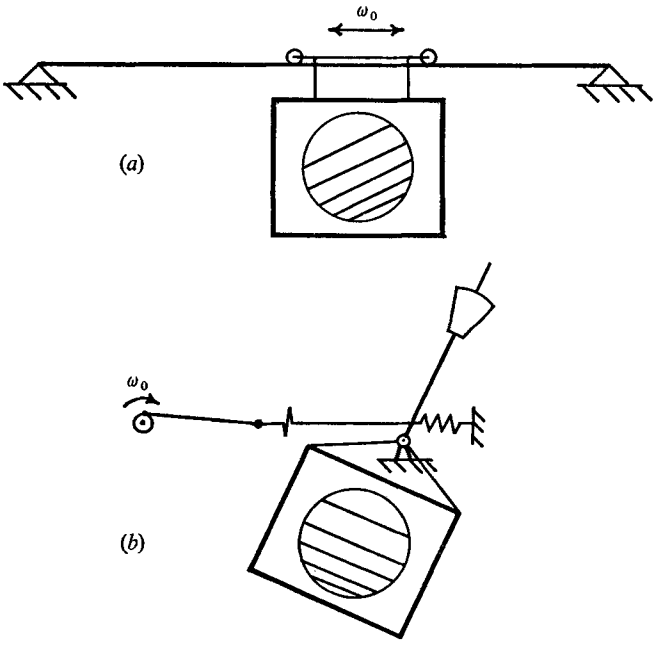

FIGURE 4. Methods of forcing. (*a*) Horizontal method. (*b*) Pendulum method.

quickly, then decayed as the basic oscillation diminished in amplitude. By careful timing, that oscillation could be sustained at a moderately steady level by repeated movement of the frame through smaller distances.

Steadiness was not the main problem with this method, however. Because the cylindrical walls did not move with the fluid, a periodic boundary layer was formed on them. From (2.22), the thickness scale of this layer depended upon the angle of the wall, and became large as this angle approached the characteristic angle $\arccos \omega_0/N$, in this case approximately $\frac{1}{4}\pi$. By virtue of its displacement effect, therefore, the cylindrical boundary layer was a strong generator of wave modes of basic frequency ω_0, which tended to swamp the effects sought. In addition the layer was subject to instabilities (now being studied separately) tending to produce intrusive mixing.

These undesirable effects were eliminated in the second method (II) of forcing the basic oscillation, in which the whole assembly was suspended from a horizontal pivot 33·5 cm directly above the cylindrical chamber axis (see figure 4*b*). A heavy counterweight above the pivot made the assembly into a compound pendulum whose period could be adjusted to correspond roughly to that of the basic internal mode. A stiff flexible linkage (a long steel cable) connected the pendulum to a crank driven through a gearbox by an infinitely variable, precisely speed-controlled d.c. motor.

With careful adjustment of the crank throw and speed, the swing of the assembly could be synchronized precisely with the liquid inside the cylindrical cavity, so that negligible relative movement occurred, and the boundary-forced modes and mixing disappeared. Unstable modes took a great deal longer to

develop, but since the swing amplitude was constant and could be accurately adjusted, it was possible to determine with precision the critical amplitude below which instabilities vanished.

4. Results

4.1. *Visualizations*

Figures 5 and 6 (plates 1–5) are a selection of schlieren photographs of the development of parametric instability using the horizontal and pendulum forcing methods described in the previous section. For all of these the image of a knife-edge obscuring the lower half of a diffused quartz–iodine–tungsten source (about 4 cm^2 in diffuse area) was refocused on a knife-edge within a 1 cm circular aperture. The system was effectively sensitive only to components of the density gradient normal to the edge. The chamber image was refocused within a 35 mm camera body. Close examination of the figures shows a regular fine-scale diagonal pattern probably caused by polishing marks in the plate-glass chamber ends. The small black dots are neutrally buoyant beads used for determining the basic mode amplitude.

Figure 5 (*a*) shows the image, with a vertical knife-edge, 15 s after method I forcing of the basic solid-body rotation mode to an amplitude $\alpha_M(t = 0)$ of about 5°. The period of this mode was 10 s. The cylindrical boundary layer was laminar and the boundary-layer-forced (cross) mode was visible, aligned at $\pm 45°$. No other modes were detected. Figure 5 (*b*) was taken under the same conditions but with an $\alpha_M(t = 0)$ of about 15°. The boundary layer had become turbulent and the cross-mode was stronger. Figure 5 (*c*) was taken 50 s later and clearly shows the presence of another mode of shallower angle. In figure 5 (*d*), taken after another 50 s, that mode was attenuating but delineated modes with a well-defined characteristic angle of 20°. Figure 5 (*e*) was taken after the development of instability under the same conditions as above, but with an $\alpha_M(t = 0)$ of about 20°. In this case, finer-scale structure had developed and there were evidently 'traumata' or intense irreversible distortions of the density field.

Figures 6 (*a*) and (*b*) were taken during method II forcing. The oscillation period was 14·6 s with a horizontal schlieren cut-off. Figure 6 (*a*) shows a well-developed instability with a pendulum amplitude α_M of 14°. The characteristic angle is about 19°. After this photograph was taken, α_M was reduced to 8·5°, where the instability decayed and disappeared. Figure 6 (*b*) was then taken, and shows only very weak evidence of a boundary-layer-generated cross-mode. Because of the horizontal schlieren cut-off the density-gradient defects near top and bottom can be seen clearly.

4.2. *Measurement of critical amplitude*

Using method II, the pendulum method, the critical angle for sustaining the unstable mode could be determined with precision, using frame-by-frame analysis of a 16 mm cine film of trajectories of neutrally buoyant particles. However, some caution is needed in interpreting the results as a reliable verification

of the mechanism of parametric instability, and for this reason the procedure will be given here in some detail.

The natural frequency ω_0 of the basic solid-body rotation mode could be measured to within $\pm 0{\cdot}1\,\%$. If the stratification were completely uniform this would give the buoyancy frequency of the liquid inside the cylindrical chamber, since then $N = 2^{\frac{1}{2}}\omega_0$. In non-uniform stratification, ω_0 is related to the density distribution $\rho(z)$ through the following compound-pendulum relations:

$$\left.\begin{aligned} &\omega_0^2 = -g\epsilon/\kappa^2, \quad \theta = \arcsin z/a, \\ &\tau = \int_{-\frac{1}{2}\pi}^{\frac{1}{2}\pi} \rho(z/a)\cos^2\theta\, d\theta, \quad \epsilon = \frac{a}{\tau}\int_{-\frac{1}{2}\pi}^{\frac{1}{2}\pi} \rho \sin\theta \cos^2\theta\, d\theta, \\ &\kappa^2 = \frac{a^2}{\tau}\int_{-\frac{1}{2}\pi}^{\frac{1}{2}\pi} \rho\cos^2\theta\,(\tfrac{1}{3}\cos^2\theta + \sin^2\theta)\, d\theta. \end{aligned}\right\} \tag{4.1}$$

$\rho(z = +a)$ was known to sufficient accuracy, and by micrometer traversing of the schlieren knife-edge it was possible to calibrate† the apparatus and determine $\rho'(z) - \rho_c'$, where the latter term is the (inaccurately known) constant static density gradient within the central region of the chamber. $\omega_0(\rho_c')$ was derived by substituting trial values of ρ_c' in the above equations, and interpolation to the measured ω_0 then gave the true ρ_c' and a complete $\rho'(z)$ profile.

The importance of knowing this profile was that it allowed the frequency of possible free cylindrical modes to be determined more precisely than was possible by direct measurement. As indicated by (2.7), free modes of constant frequency ω require complete closure of rays at the characteristic angle β to the vertical given by the dispersion relation

$$\beta(z) = \begin{cases} \arccos(\omega/N(z)), & \omega < N(z), \\ 0, & \omega > N(z), \end{cases} \tag{4.2}$$

where

$$N^2(z) = -g\rho_0'(z)/\rho(z). \tag{4.3}$$

From an experiment giving the results to be discussed below, the density profile was determined by the above techniques, and representative ray trajectories were calculated by integration of (4.2). These are shown in figure 7. The pendulum frequency ω_0 was $0{\cdot}5894 \pm 0{\cdot}0003\,\mathrm{s}^{-1}$, and the rays illustrated were the low wavenumber modes whose frequency ω, as defined by (4.2) above, came closest to the value $\frac{1}{2}\omega_0$, viz. $0{\cdot}276 \pm 0{\cdot}0002\,\mathrm{s}^{-1}$.

For the mode identified the viscous damping rate κ^* was calculated from (2.22) and (2.24)–(2.27), making the justifiable assumption that, owing to the insensitivity of κ^* to l, N could be taken as constant and equal to $2^{\frac{1}{2}}$ times the observed pendulum frequency, and that the mode in question had a β value of about $\frac{3}{8}\pi$.

Replacing the term $\frac{1}{4}\nu^2k^4(1+l^2)$ by $\kappa^{*2}(1+l^2)$ in (2.14), the coefficient A was determined. The intersection of this A with the contour $e^{i\mu\pi} = e^{2\kappa\pi/\omega_0}$ in figure 1 then gave the predicted value for Q and thus from (2.14) the predicted α_M for instability.

† Direct calibration gave the required value of $\partial n/\partial\rho$, the refractive-index/density gradient, $0{\cdot}2405\ \mathrm{cm^3\,g^{-1}}$ (cf. Mowbrays' (1967) value of 0·231).

	Condition	α_M and standard deviation	$\beta(\lvert z\rvert < 0{\cdot}7a)$
Pendulum experiment $\omega_0 = 0{\cdot}5891\ \mathrm{s}^{-1}$	Disturbance mode could be sustained indefinitely at a level perceptible using schlieren technique at maximum sensitivity	$7{\cdot}055°$ $\sigma = 0{\cdot}086°$	$70{\cdot}85$ $\sigma = 1{\cdot}17°$
	Disturbance mode decayed and became imperceptible	$6{\cdot}67°$ $\sigma = 0{\cdot}056°$	
Theory	Using procedure outlined in text	$6{\cdot}95°$	$70{\cdot}77°$

TABLE 1

For the experiment with the profile given in figure 6 the results in table 1 were obtained.

The experimental values were derived from the measured excursions of several neutrally buoyant particles over two cycles of oscillation under steady conditions maintained over about 100 cycles. In the unstable case averaging over two cycles minimized the movement due to the unstable mode. Experimental β's were taken from the cine record of a well-developed instability,† filmed prior to the test for determination of the critical α_M.

Agreement with theoretical predictions for both α_M and β is remarkably good and this substantially confirms the mechanism of parametric instability. It will be appreciated from figure 1 that the sensitivity of μ to A and Q (and thus, of α_M to ω/N) for growth factors $e^{i\mu\pi}$ near unity in the vicinity of $A^{\frac{1}{2}} = 1$ made the foregoing procedure for the determination of $A^{\frac{1}{2}}$ necessary for accurate verification.

Further confirmation was found from the observed phase of the disturbance mode relative to the forcing oscillation. This was not measured precisely, but as well as could be judged from the cine records the nodes in ρ lead the nodes in α by $31{\cdot}5° \pm 3°$ for a weak but detectable instability.

From Rhines (1970, equation (6)), the Floquet solution to (2.13), represented in the form

$$S(s) = \exp(i\mu s) \sum_{n=-\infty}^{\infty} C_n \exp(2ins),‡$$

has, in the vicinity of the primary resonance $O(\mu - 1) \leqslant Q$, only two dominant terms, whose coefficients are related by

$$C_{-1}/C_0 = \sigma/Q.$$

σ is defined as $A - \mu^2$, and is determined from the defining variables through the relation

$$A = 1 + (\mu - 1)^2 \pm [4(\mu - 1)^2 + Q^2]^{\frac{1}{2}}.$$

† Though revealed clearly by schlieren photographs, the dimensionless amplitude $\Delta\rho m/\rho'_{00}$ was never greater than about 0·1, where $\Delta\rho$ is the maximum vertical density perturbation.

‡ Our μ corresponds to Rhines' m.

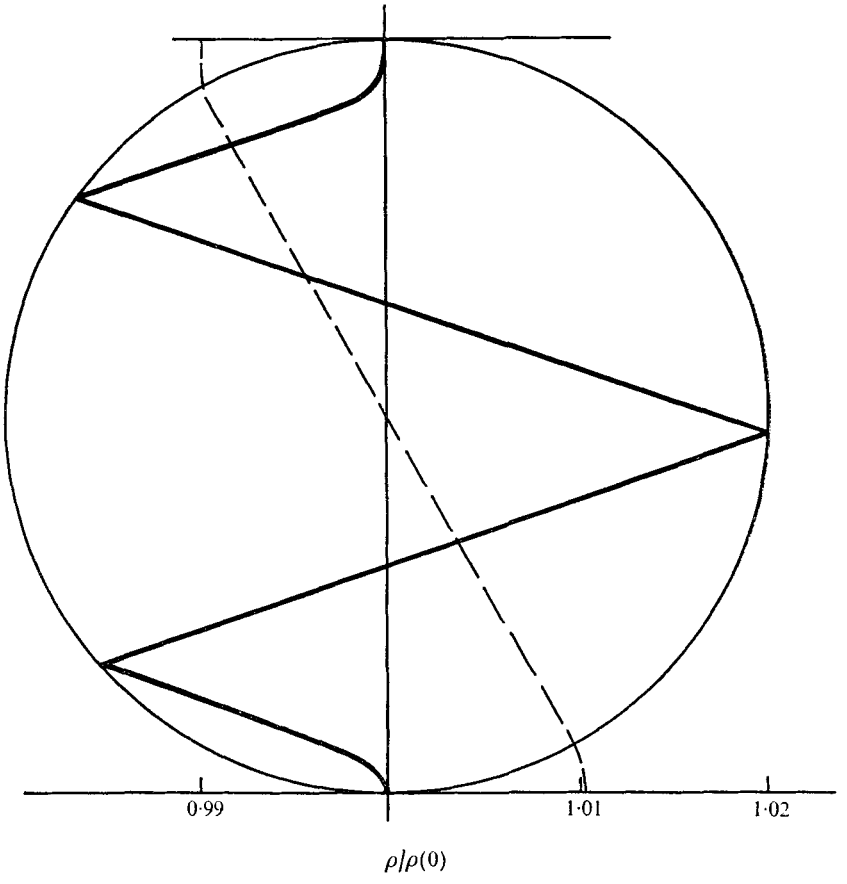

FIGURE 7. Density profile and closing characteristic ray trajectory for measurement of critical amplitude α_M.

For the present experimental conditions the last expression cannot be satisfied, and A lies within the 'stopping band' $1-Q < A < 1+Q$ for which $\mu = 1$. Within the band solutions are admitted only for modes whose node, given by C_{-1}/C_0, is at

$$S_0 = \tfrac{1}{2}\arg[-\hat{\sigma}/Q + i(1+\hat{\sigma}/Q^2)^{\frac{1}{2}}],$$

where $\hat{\sigma} = A - 1$ (see Rhines 1970, §5).

For the results tabulated above $A = 0{\cdot}8803$ and $Q = 0{\cdot}1443$, thus $S_0 = 16{\cdot}97°$, which leads the node in α by 28·03°, comparing well with the above observed value.

Similarly good agreement was obtained in other experiments, but less precise methods of measuring α_M and $\rho'(z)$ introduced ambiguities weakening the validity of the results, so these results will not be given here.

5. Evidence of parametric instability from previous experiments

In photographs taken during previously reported experiments on internal waves in a continuous stratification (McEwan 1971, 1973) there is found to be evidence of localized parametric instability. Figure 8 (*a*) (plate 6) is an enlargement of a shadowgraph in the same sequence as figure 6 of McEwan (1971), and was taken at about time (*f*) of that sequence. The arrows indicate a series of parallel diagonal distortions in the density field. These are distinguishable from the dyed isopycnal surfaces, which show large-scale modulation resulting from resonant interaction. Their shallow angle to these surfaces and their regularity and symmetry within the background motion all suggest that the distortions are the development of a parametric instability upon the forced mode. This mode had a characteristic angle $\arcsin \omega/N$ (to the horizontal) of 30°, and a half-frequency mode would then have had an angle of $\arcsin \omega/2N = 14{\cdot}5°$. As indicated on the figure, this is close to the observed angle.

Figure 8 (*b*) (plate 7) shows a similar magnification of a shadowgraph belonging to a sequence part of which is published in Turner (1973, plate XXIV) of a standing wave in which low-order resonant interaction does not take place. Again, diagonal distortions can be detected. In this case their angle (about 10°) to the local isopycnal surface slightly exceeds the half-frequency angle (about 8°).

A third example is shown in two stages (figures 8 *c, d*, plates 7, 8), separated in time by about 1 min or 9·3 'buoyancy periods' $2\pi/N$. Two internal wave beams were projected from the top corners of a rectangular tank (see McEwan 1973). The axes of these beams are indicated by diagonal solid lines on the figures. The figures are shadowgraphs, and the smaller dark spots are suspended liquid droplets, used for motion measurement. As can be seen, there was a rapid development of a region of density disturbance along a diagonal direction at a lower angle than either of the rays. If this were the result of the dispersion of free modes generated somehow through the interaction of the forced beams these modes would have a characteristic angle of 9·8° to the horizontal. This is shown as a broken line on figure 8 (*c*), evidently shallower than the disturbances beyond the interaction region, where the solid lines cross. The angle for half-frequency parametric instabilities developing on the right-hand beam, $\arcsin \omega_{\text{right}}/2N$, is 14·8°. This is shown in figure 8 (*d*) to correspond closely to the observed disturbance angle (unlike the example of figure 8 (*a*) the angle is drawn relative to the horizontal, since the isopycnal slope is comparatively small, and non-uniform in space; the right-hand wave beam had a horizontal wavelength of 30·5 cm; the grid on figures 8 (*c*) and (*d*) is 10 cm square).

A notable feature of the foregoing observations was that in each case the appearance of these fine-scale shallow distortions was an immediate harbinger of '*traumata*', irreversible layering intensifications of discontinuities in the density gradient. Furthermore, an observed coincidence of scale and location indicates that they were generators of these traumata. Hence there is a strong suggestion that parametric instability is an important direct mechanism for the creation of layered structure in a continuous stratification under the action of internal waves.

6. Application to the oceanic thermocline

The foregoing observations lead naturally to the question of whether parametric instability is a potentially important dynamical process in the ocean and atmosphere. Since oceanic internal wave spectra are the better known, it is to these that attention is directed here.

Garrett & Munk (1972*a*) derived and fitted to observations a horizontally isotropic internal wave energy spectrum. They then used this (Garrett & Munk 1972*b*, referred to as GM) to estimate mixing by shear instability. Their proposal that shear instability and not overturning, as suggested by Orlanski & Bryan (1969), produced most mixing was based on the result that the unit isopycnal slope was 38 times the r.m.s. slope predicted using their spectrum, while a Richardson number of $\frac{1}{4}$ was reached with only $5{\cdot}7(N(z)/N_T)^{-\frac{1}{2}}$ r.m.s. shears, where N_T is the buoyancy frequency at the top of the thermocline.

From equation (3.1) of GM the expression for the mean-square slope is, in our notation (with an asterisk indicating non-dimensional quantities),

$$\overline{\alpha}^2 = \frac{2\omega_i^*}{j_i \pi^2} E N^{*-1} \int_{\omega_i^*}^{N^*} \int_0^J k^{*2} \omega^{*-3} \, dk^* \, d\omega^*, \tag{6.1}$$

where ω_i^* is the local inertial frequency, E is a constant, j_i defines the number of modes for which E is fitted to spectra data and J is the wavenumber range, limited to

$$J = j_i \pi (\omega^{*2} - \omega_i^{*2})^{\frac{1}{2}}. \tag{6.2}$$

Substituting,

$$\overline{\alpha}^2 = \frac{2\omega_i^* E j_i^2 \pi}{3N^*} \int (\omega^{*2} - \omega_i^{*2})^{\frac{3}{2}} \omega^{*-3} \, d\omega^*, \tag{6.3}$$

so that, except for frequencies near to ω_i^*, the integrand is virtually constant. In a continuous spectrum the contribution to the mean-square slope from a bandwidth $\Delta\omega^*$ is proportional to $\Delta\omega^*$.

We need to know whether a given internal wave mode can be parametrically amplified in the presence of a spectrum of waves producing the above slopes. If the spectrum were truly continuous the equation for solution would be, at its simplest, of second order with random continuous coefficients, obviously beyond the scope of the present study. However, progress is possible with the reasonable proposition that, at any single place and time in the thermocline, the spectrum, or large-scale parts of it, is dominated by a finite, possibly small number of wave modes. Each of these modes, provided that it remains coherent for several cycles, is independently capable of parametrically exciting finer-scale waves of approximately half the frequency. Conversely, a fine-scale model is liable to energization by trains of large-scale waves of appropriate, nearly double frequency. Over a narrow bandwidth $\Delta\omega_0^*$, the component of the r.m.s. *maximum* slope (in a given vertical plane containing the vector wavenumber of the mode being parametrically amplified) might then be, on average, from (6.3),

$$\overline{\alpha}_{\mathrm{J}f_0} = (2\omega_i^* \pi E j_i^2 / 3N^*)^{\frac{1}{2}} \Delta\omega_0^*, \tag{6.4}$$

on the assumption that $\bar{\alpha}_{M_0}$ in a given direction equals the r.m.s. slope amplitude averaged over two directions.

Consider $\Delta\omega_0^*$ to be defined as the bandwidth for unstable parametric forcing of a single mode (denoted by a subscript 2). For simplicity only the contribution from frequencies near $2\omega_2^*$ are taken, the others being much smaller. With the definitions given in (2.14) and neglecting the small viscous term in A, an average value of $2Q/A$ is defined:

$$2Q/A = \bar{\alpha}_{M_0} l_2, \tag{6.5}$$

where $l_2 \equiv m_2/k_2$. The Floquet solutions, figure 1, give

$$f(2Q/A, i\mu, A^{\frac{1}{2}}) = 0,$$

where $A^{\frac{1}{2}} \equiv 2\omega_2/\omega_0$. $\omega_2(l_2)$ is given by the dispersion relation of GM, equation (2.4),

$$l_2 = N/(\omega_2^2 - \omega_1^2)^{\frac{1}{2}}, \tag{6.6}$$

which differs from (2.7) through the effects of rotation and stratification non-uniformity.

For an individual mode subjected to viscous damping, growth occurs when the condition (2.18) is satisfied, i.e. for a specific mode

$$\mathrm{Re}\,(i\mu\omega_0) > \nu k_2^2(1 + l_2^2). \tag{6.7}$$

For an ensemble of modes, encompassing a bandwidth $\Delta\omega_0$, the left-hand side is replaced by a value averaged over this bandwidth, i.e.

$$\mathrm{Re}\,\overline{(i\mu\omega_0)} = \frac{4\omega_2^{*2}}{\Delta\omega_0^*} \int^{\Delta(A^{-\frac{1}{2}})} \mathrm{Re}\,(i\mu A^{-\frac{1}{2}})\, d(A^{-\frac{1}{2}}),$$

where $\Delta(A^{-\frac{1}{2}}) = [\omega_0(i\mu = 0, A < 1) - \omega_0(i\mu = 0, A > 1)]/2\omega_2 = \Delta\omega_0/2\omega_2$.

The value of this integral is found as a function of $2QA^{-1}(\Delta\omega_0/2\omega_2)^{-\frac{1}{2}}$; by graphical integration, the following empirical relation is determined:

$$\mathrm{Re}\,\overline{(i\mu\omega_0)}/2\omega_2 \sim 0{\cdot}113(2QA^{-1}(\Delta\omega_0/2\omega_2)^{-\frac{1}{2}})^{2{\cdot}12} \quad \text{as} \quad Q \to 0. \tag{6.8}$$

Wavenumbers and frequencies were scaled by GM using $7{\cdot}665 \times 10^{-6}$ rad cm^{-1} and $5{\cdot}23 \times 10^{-3}$ rad s^{-1}, these being appropriate to a buoyancy depth scale of 1·3 km and a maximum buoyancy frequency of 3·0 cycles per hour. ω_i was taken as 0·0133 (lat 28·6°) and the GM spectrum was fitted with $j_i = 20$ and $E = 2\pi \times 10^{-5}$.

Let the vertical wavenumber of the unstable mode be m_2 $(= l_2 k_2)$. Then substituting (6.4)–(6.6) into (6.8), and replacing $\mathrm{Re}\,\overline{i\mu\omega_0}$ on the left-hand side of (6.7), modes will be unstable if

$$m_2 < 0{\cdot}145N^{*2{\cdot}06}\omega_2^{1{\cdot}03}(\omega_2^{*2} - \omega_i^{*2})^{-1{\cdot}06}(N^{*2} + \omega_2^{*2} - \omega_i^{*2})^{-\frac{1}{2}}. \tag{6.9}$$

At the higher frequencies $N^* \gg \omega_2^* \gg \omega_i^*$, this becomes

$$m_2 < 0{\cdot}145N^{*1{\cdot}06}\omega_2^{*-1{\cdot}09}\ \mathrm{cm}^{-1},$$

and for $\omega_2^* = \omega_i^* + \Delta\omega^* \sim \omega_i^*$

$$m_2 < 0{\cdot}039N^{*1{\cdot}06}(\Delta\omega^*)^{-1}\ \mathrm{cm}^{-1}.$$

The coefficient in the last expression is reduced through the drop in the integrand of (6.3) as $\omega^* \to \omega_i^*$.

From the above, even admitting possible inaccuracies amounting to an order of magnitude in both the spectrum definition and the present simplified treatment, it seems very likely that parametric instability might be excited in modes with vertical wavelengths down to tens of centimetres. Finest-scale instability is favoured in the *lowest frequency* modes and should be most common where N^* is a maximum.

This susceptibility is not intended to suggest that parametric instability is a significant *direct* cause of oceanic mixing. Shear and overturning instabilities are still likely to be the ultimate mechanisms. It is seen, rather, as an effective means for cascading energy to lower frequencies and larger vertical wavenumbers, with the distinction from its genus, *resonant interaction*, that with the spatial wavenumbers sufficiently widely separated in magnitude, the process becomes insensitive to the forcing wavenumber.

A potential criticism of the foregoing treatment is that it effectively considers time averages of the amplitude at a point, while in a real system (extensive or unbounded), the dispersion of a group of fine-scale waves forced by a given excitation event would rapidly attenuate the group. In answer it is noted that the group velocity of the large-scale waves is greater by a factor roughly proportional to the ratio of the vertical wavelengths of the large and fine waves, and also that the spatial extent of a large-scale wave group is likely to be greater; thus the latter engulfs and 'outruns' the fine-scale group, and provides a spatially averaged forcing equivalent to time averaging, notwithstanding dispersion. The 'spreading' of traumata along the right-hand internal wave beam as shown by comparing figures 8 (*c*) and (*d*) provides some evidence that dispersing waves can continue to derive energy from a large-scale field.

In the oceanic context, then, the process is visualized as follows: groups of fine-scale waves of low frequency are advected by the field of larger waves, and are energized whenever this field contains a coherent group of substantially larger wavelength and a frequency within the forcing bandwidth. Because the growth-rate coefficient is exponential, there is a tendency to sustain pre-existing structure. If amplitudes grow large enough, irreversible traumatic distortion of the density field of the kind detected in experiments might occur, producing a layered structure of the same scale. Conversely interaction of this layered structure with the large-scale field could conceivably produce internal wave modes for its own perpetuation.

Such possibilities do not conflict with observed oceanic fine-structure. Osborn & Cox (1972) found vertical temperature-gradient fluctuations down to a scale of centimetres, with highest intensities in regions where N^* was locally greatest. These conform with the predictions of (6.9) for $\omega_2^* \simeq \frac{1}{2}N^*$, which give a minimum vertical wavelength $2\pi/m_2$ of 21 cm. The frequency spectrum of the fine scales is not determinable, but, as Osborn & Cox note, the diffusion time scale is of order $2\pi/N$. If diffusion is presumed to truncate the spectrum when

$$\frac{2\pi}{m_2} = \left(4k'\frac{2\pi}{\omega_2}\right)^{\frac{1}{2}},$$

where k', the thermal diffusivity, is $0{\cdot}0014\,\mathrm{cm^2\,s^{-1}}$, then substituting in (6.9), the vertical wavelength minimum at truncation is

$$\lambda_2 = 2\pi/m_2 > 8{\cdot}07N^{*-\frac{1}{3}}$$

or with $N^* \simeq 3{\cdot}6$, appropriate to Osborn & Cox's observed local high gradient regions, $\lambda_2 > 5{\cdot}2\,\mathrm{cm}$, for which $\omega_2^* \simeq 0{\cdot}5$. In other words the minimum predicted wavelength is close in magnitude to the finest structure observed, it diminishes with increasing N^* and the cut-off frequency is not greater than the mean maximum buoyancy frequency, and is an order of magnitude lower than local maxima.

7. Concluding remarks

Parametric instability in stably stratified media, regarded as a member of a class of wave interaction phenomena, is evidently an important one. For its occurrence at realistic disturbance levels, the limitations on the frequency range for either the forcing wave or the unstable mode are not stringent. Furthermore, the requirement for the presence of three modes of appropriate wavenumber and frequency in the case of resonant interaction is relaxed when the wavelength of the forcing mode is larger to a 'sufficient' degree than that of the unstable mode.

The previous experiments (§5) indicate that the 'sufficient' scale difference is about an order of magnitude but the present simple theory gives no more precise definition. It can be seen from the basic equations (2.1) and (2.2) that retention of spatial derivatives for both modes increases considerably the complexity as well as the order of the resultant growth equation and solution is not straightforward.

By avoiding as well as possible the above limitation and the likelihood of resonant interaction, the present experiments confirmed the predictions of simple theory. For practical reasons the experiments did not cover a wide range of defining variables, but the one quantitative result was unequivocal.

From the content of §6 the process appears to be worthy of further attention in its application to the formation and maintenance of wavy microstructure in the ocean and atmosphere. Apart from the observations of §5 no direct connexion has been established between the occurrence of irreversible distortion and mixing and the emergence of the instability, but there is little doubt that in its presence the susceptibility to small-scale static and shearing instabilities is increased. In the atmosphere, larger-scale vertical structure might also be parametrically sustained by mesoscale baroclinic effects of a quasi-periodic nature, such as sea breezes and fronts. Furthermore, the gross similarity between internal waves and other geophysical finite amplitude wave phenomena, notably inertial, Rossby and baroclinic waves, leads one to speculate that the mechanism may have other, more general applications.

The close collaboration and advice of Dr P. G. Baines throughout the course of this work is gratefully acknowledged.

REFERENCES

ABRAMOWITZ, M. & STEGUN, I. A. 1965 *Handbook of Mathematical Functions*, §20, pp. 722–730. Washington: Nat. Bur. Stand.

BARCILON, V. 1968 Axi-symmetric inertial oscillations of a rotating ring of fluid. *Mathematika*, **15**, 93–102.

BENJAMIN, T. B. & URSELL, F. 1954 The stability of a plane free surface of a liquid in vertical periodic motion. *Proc. Roy. Soc.* A **225**, 505–515.

BOWEN, A. J. & INMAN, D. L. 1969 Rip currents 2. Laboratory and field observations. *J. Geophys. Res.* **74**, 5479–5490.

BRILLOUIN, L. 1953 *Wave Propagation in Periodic Structures*. Dover.

GARRETT, C. J. R. 1970 On cross-waves. *J. Fluid Mech.* **41**, 837–849.

GARRETT, C. & MUNK, W. 1972*a* Space-time scales of internal waves. *Geophys. Fluid Dyn.* **3**, 225–264.

GARRETT, C. & MUNK, W. 1972*b* Oceanic mixing by breaking internal waves. *Deep-Sea Res.* **19**, 823–832.

MCEWAN, A. D. 1971 Degeneration of resonantly-excited standing internal gravity waves. *J. Fluid Mech.* **50**, 431–448.

MCEWAN, A. D. 1973 Interactions between internal gravity waves and their traumatic effect on a continuous stratification. *Boundary Layer Met.* **5**, 159–175.

MCEWAN, A. D., MANDER, D. W. & SMITH, R. K. 1972 Forced resonant second-order interaction between damped internal waves. *J. Fluid Mech.* **55**, 589–608.

MAHONY, J. J. 1972 Cross-waves. Part 1. Theory. *J. Fluid Mech.* **55**, 229–244.

MARTIN, S., SIMMONS, W. & WUNSCH, C. 1972 The excitation of resonant triads by single internal waves. *J. Fluid Mech.* **53**, 1, 17–44.

MOWBRAY, D. E. 1967 The use of schlieren and shadowgraph techniques in the study of flow patterns in density stratified liquids. *J. Fluid Mech.* **27**, 595–608.

ORLANSKI, I. 1972 On the breaking of standing internal gravity waves. *J. Fluid Mech.* **54**, 4, 577–598.

ORLANSKI, I. 1973 Trapeze instability as a source of internal gravity waves. Part I. *J. Atmos. Sci.* **30**, 1007–1016.

ORLANSKI, I. & BRYAN, K. 1969 Formulation of the thermoclinic step structure by large amplitude internal waves. *J. Geophys. Res.* **74**, 6975–6983.

OSBORN, T. R. & COX, C. S. 1972 Oceanic fine structure. *Geophys. Fluid Dyn.* **3**, 321–345.

RHINES, P. B. 1970 Wave propagation in a periodic medium with application to the ocean. *Rev. Geophys. Space Phys.* **8**, 303–319.

TURNER, J. S. 1973 *Buoyancy Effects in Fluids*. Cambridge University Press.

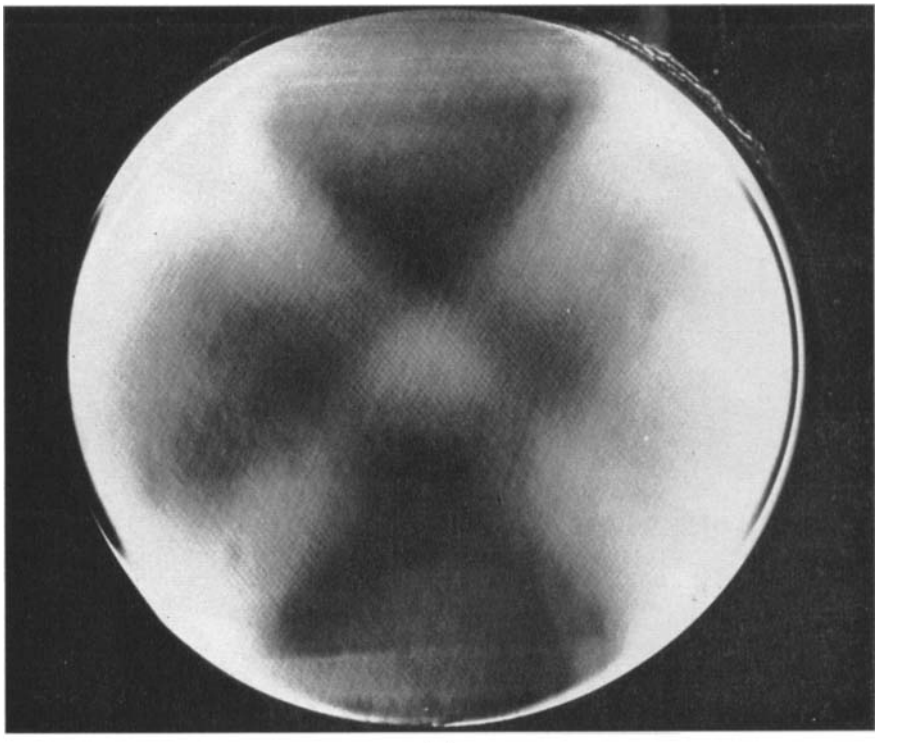

(*a*)

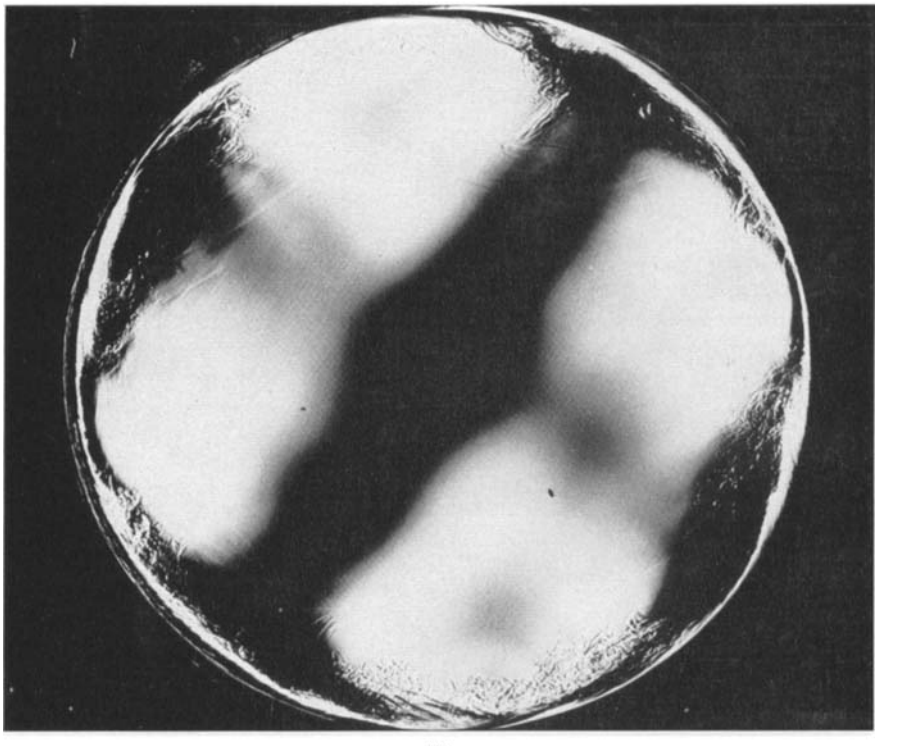

(*b*)

FIGURES 5(*a*, *b*). For caption see plate 3.

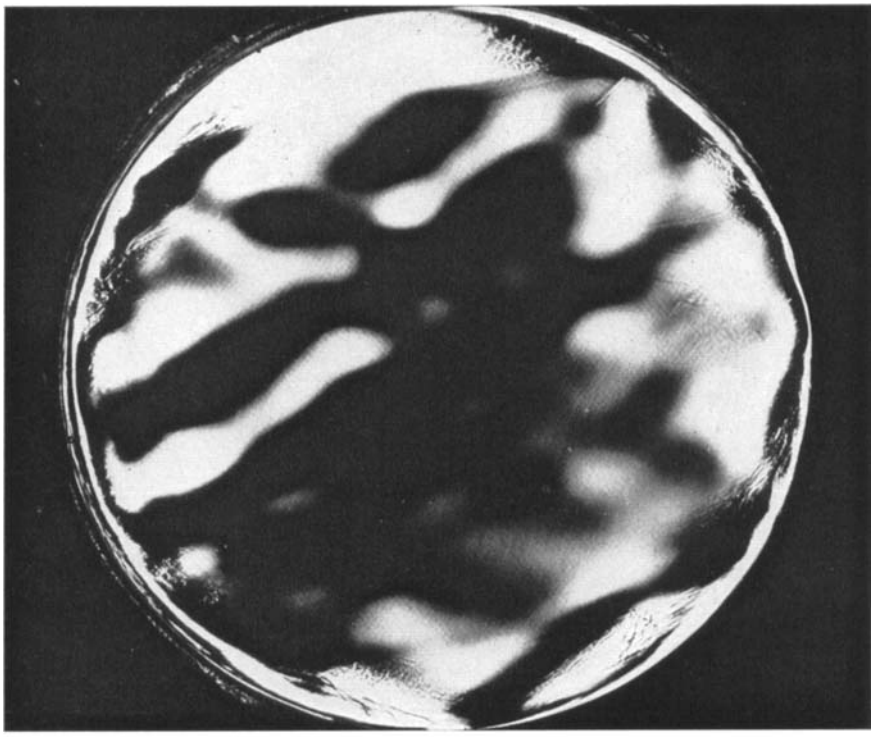

(*c*)

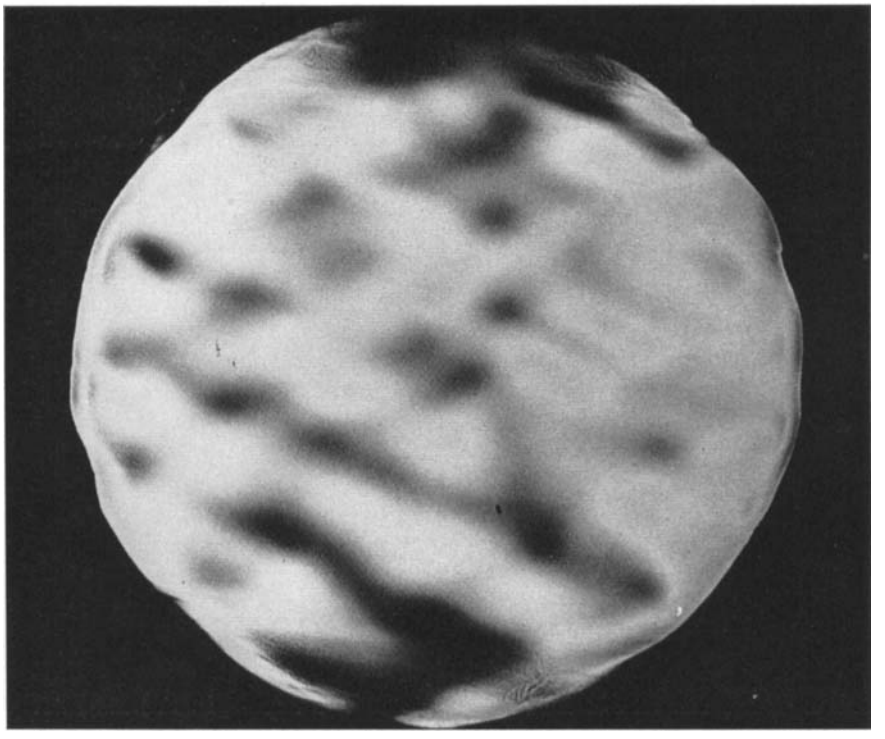

(*d*)

FIGURES 5(*c*, *d*). For caption see plate 3.

(*e*)

FIGURE 5. Schlieren observations with a vertical knife-edge, following 'horizontal' forcing. (*a*) $\alpha_M(t = 0) \simeq 5°$. No parametric instability. The 45° cross-mode is due to boundary-layer displacement effects. (*b*) $\alpha_M(t = 0) \simeq 15°$, $\omega_0 \simeq \frac{1}{8}\pi\ \mathrm{s}^{-1}$. Immediately after cessation of forcing. Cross-mode only present. Note cylindrical boundary-layer turbulence. (*c*) 50 s after (*b*). Parametric instability clearly present. (*d*) 50 s after (*c*). (*e*) $\alpha_M(t = 0) \simeq 20°$ after full development of the instability.

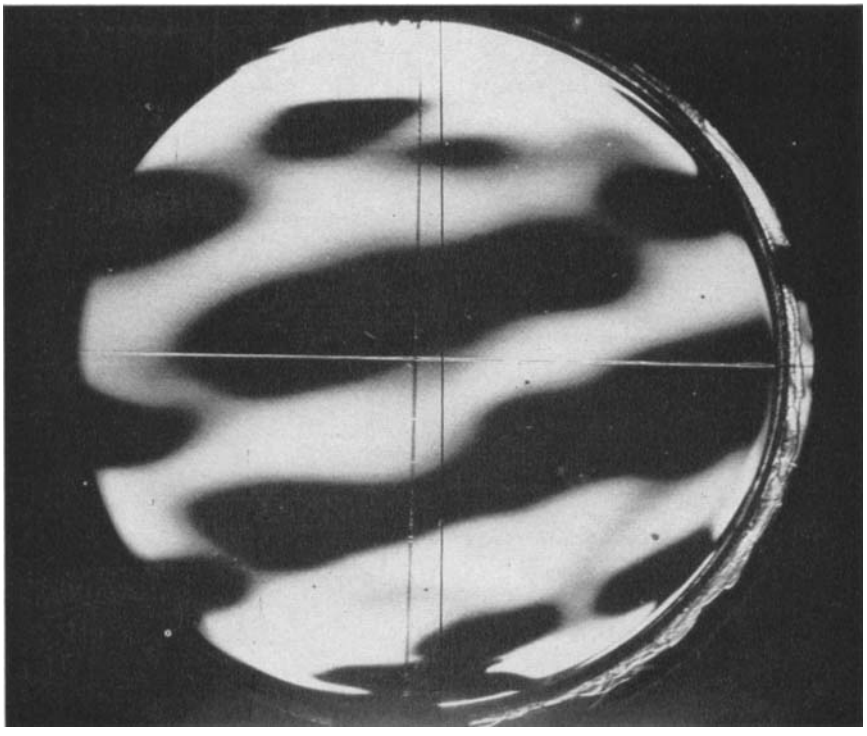

FIGURE 6(*a*). For caption see plate 5.

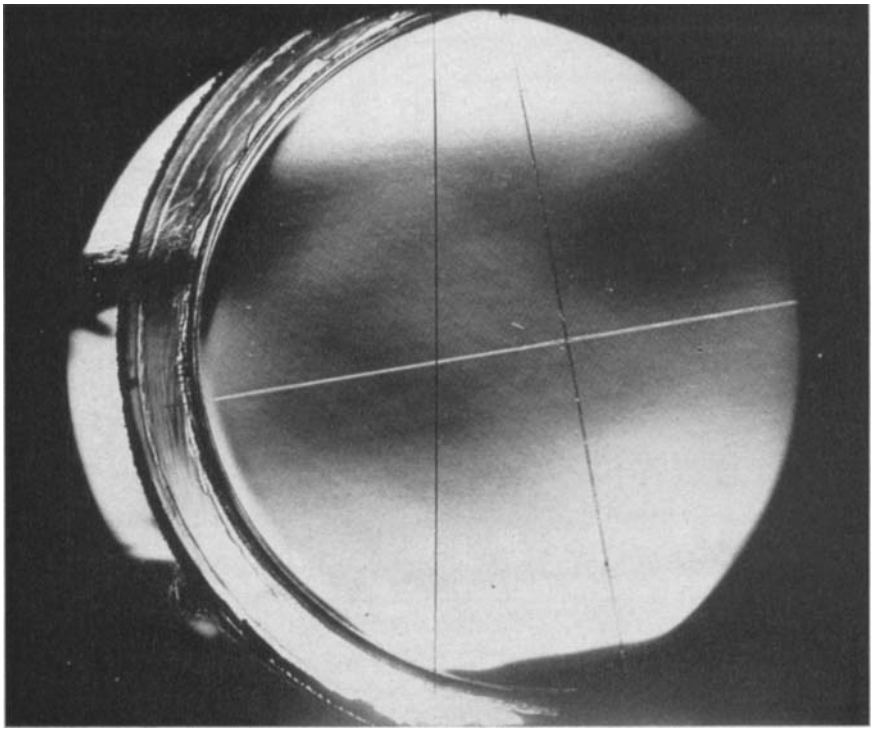

(*b*)

FIGURE 6. Schlieren observations with a horizontal knife-edge, during sustained 'pendulum' forcing. (*a*) $\alpha_M = 14°$, well-developed instability. (*b*) $\alpha_M = 8{\cdot}5°$, instability undetectable. Horizontal knife-edge at maximum sensitivity reveals density-gradient defects. Note the virtual absence of cross-modes.

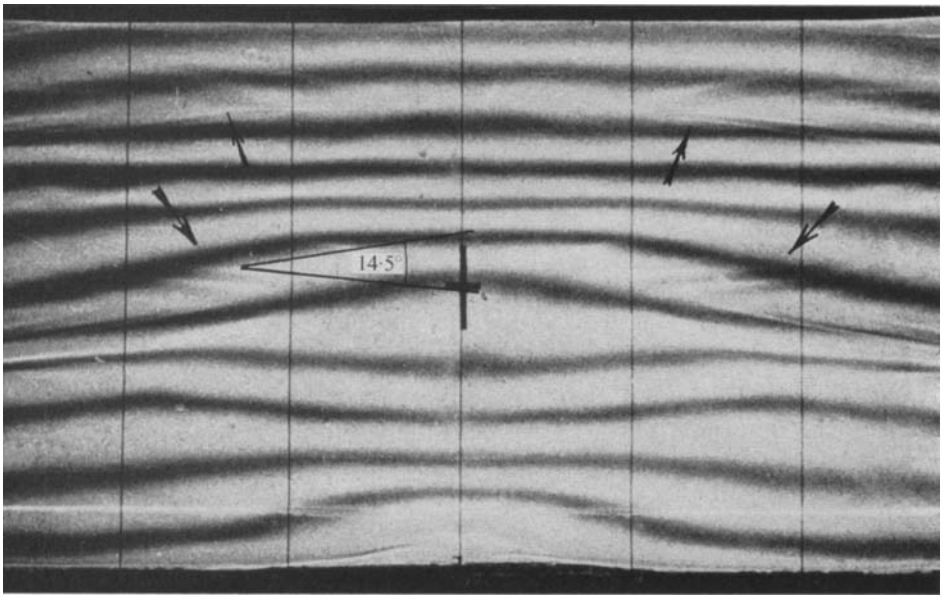

FIGURE 8(*a*). For caption see plate 8.

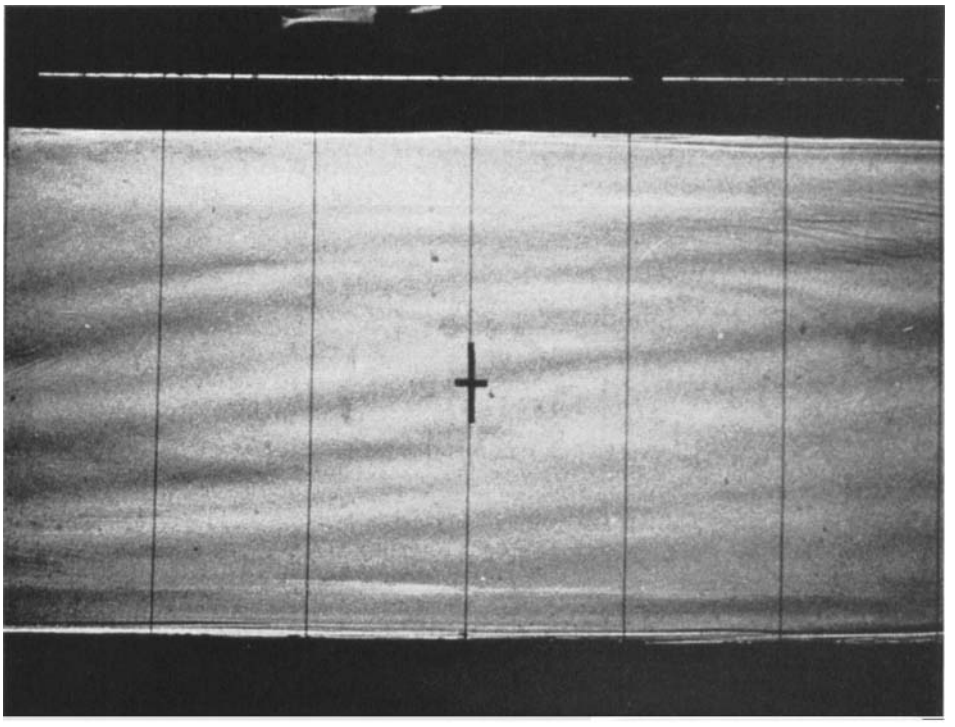

(*b*)

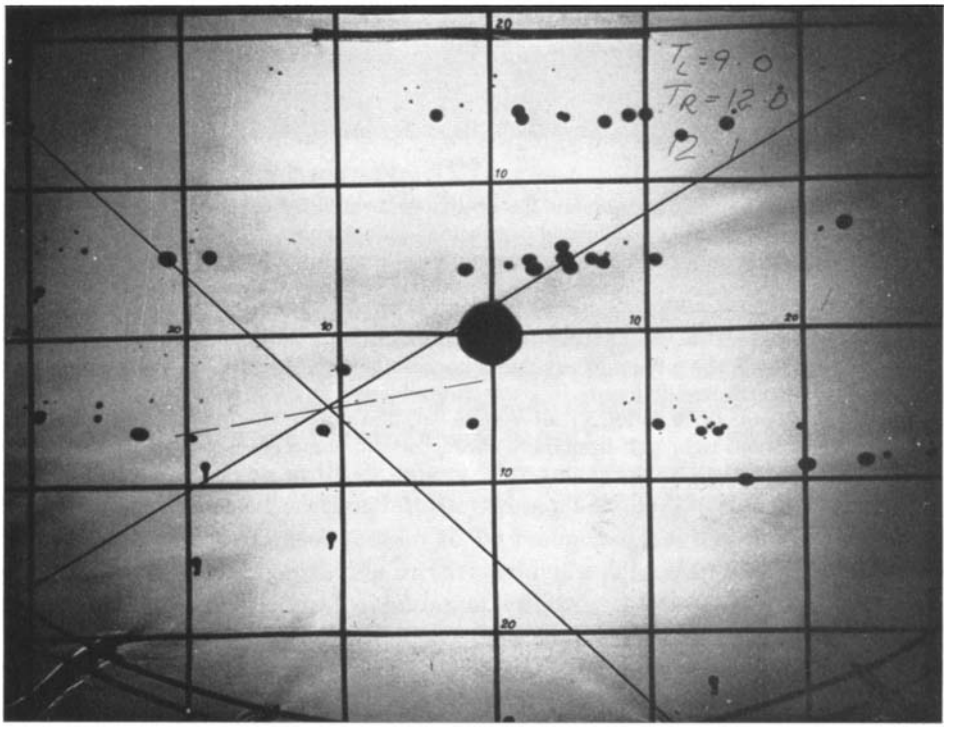

(*c*)

FIGURES 8(*b*, *c*). For caption see plate 8.

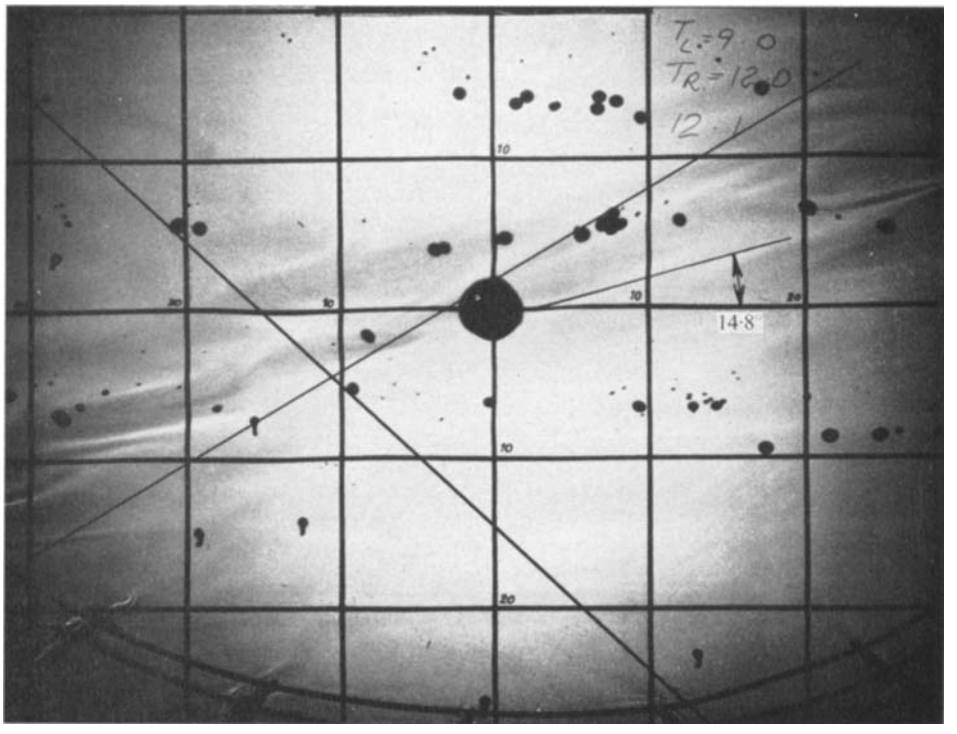

(*d*)

FIGURE 8. (*a*) Evidence of parametric instability generated by large-scale standing waves. This figure, a shadowgraph, is enlarged from the sequence given in McEwan (1971, figure 6). Tank depth is 32·6 cm. (*b*) Signs of parametric instability immediately preceding traumatic breakup of a large-scale standing wave. Figure is a shadowgraph enlargement from a sequence published by Turner (1973, plate XXIV, figure 10.5). (*c*) Shadowgraph taken during an experiment (McEwan 1973) on the interaction of crossed internal wave beams. ——, ray directions; the left-hand ray had a horizontal wavelength of 16 cm and the right-hand ray wavelength was 30·5 cm; – – –, the characteristic angle of forced interaction mode. Grid scale is 10 cm. (*d*) 9·3 ($2\pi/N$) later than (*c*). Traumatic distortions have developed along the right-hand ray; half-frequency characteristic angle (14·8°) of this ray is shown.